

Transition to the normal state induced by high current densities in $\text{YBa}_2\text{Cu}_3\text{O}_{7-\delta}$ thin films: A thermal runaway account

J. Maza,* G. Ferro, J. A. Veira, and F. Vidal

*Laboratorio de Bajas Temperaturas y Superconductividad (LBTS), Departamento de Física da Materia Condensada,
Universidade de Santiago de Compostela, E15782 Santiago de Compostela, Spain*

(Received 2 June 2008; revised manuscript received 26 June 2008; published 18 September 2008)

By using a finite-element method we analyze at a quantitative level the abrupt jump to the normal state in high- T_c films observed when measuring their current-voltage characteristics at current densities, J^* , which are between two to three times their critical current density, J_c . The experimental data that this analysis focuses on are from $\text{YBa}_2\text{Cu}_3\text{O}_{7-\delta}$ films, measured between 75 K and $T_c \approx 90$ K and under zero applied magnetic field. Our main starting point is the assumption that the constant-temperature curves, i.e., that would be measured at arbitrarily short measuring time, are smooth and so jumpless. When taking into account the finite measuring times, the highly nonlinear nature of the film's electrical conductivity, and the thermal properties of the substrate, simulation by the finite-element method shows that a thermal runaway takes place that explains, without free parameters, the experimental jumps to a 5% accuracy. The voltage values prior to the jump are also coherently accounted for with similar accuracy. No critical mechanism such as the vortex instability model from Larkin-Ovchinnikov or any others are needed for this quantitative agreement to our measurements, though they can become dominant under different refrigeration conditions, temperature range, or magnetic-field application.

DOI: [10.1103/PhysRevB.78.094512](https://doi.org/10.1103/PhysRevB.78.094512)

PACS number(s): 74.25.Fy, 74.78.Bz, 02.70.Dh

I. INTRODUCTION

The electrical transport capabilities of superconducting materials are determined by their current-voltage characteristics (CVCs), in which two current densities are especially meaningful. One is the critical current density J_c at which dissipation sets in, the other being the supercritical current density J^* at which the system is triggered into a highly dissipative state (quite close to the full normal state). This latter evolution usually takes place in an abrupt way (except very near the critical temperature T_c) signaled by a voltage jump. Because of this feature J^* is also referred to as the quench current density. Many superconducting families and topologies belonging to either high- T_c or low- T_c superconductors have been shown to exhibit a voltage jump in their CVCs. Our analysis here and experimental data will focus on $\text{YBa}_2\text{Cu}_3\text{O}_{7-\delta}$ (YBCO) thin films. Knowledge of the underlying mechanisms provoking the abrupt jump to the normal state is of fundamental interest in that it not only deepens into the superconducting state and its stability¹⁻¹⁸ but also pertains to applications because a number of superconducting devices such as current limiters¹⁹ or microstrip lines at microwaves²⁰ operate in the "limits" of their superconductivity.

The most widely accepted interpretation for the voltage jump is the flux-flow vortex instability theory by Larkin and Ovchinnikov (LO), later extended by Bezuglij and Shklovskij (BS) to include quasiparticles heating. Indeed many experimental workers may be quoted that have analyzed the voltage jump in their current-voltage (CV) curves, especially relatively near T_c , in terms of the LO or LO+BS models.¹⁻¹³

It may be pertinent for us to recall some features of the LO theory. The finite inelastic-scattering time of quasiparticles in the superconductor leads to a decreasing number of quasiparticles within a moving vortex core and to a subse-

quent viscous damping decrease. At a critical vortex velocity the differential flux-flow resistivity becomes negative. This entails that for current-biased measurement the flux-flow state becomes unstable and the superconductor switches into a highly dissipative state through a voltage jump. Thus the switch to a highly dissipative state is a *current-driven phenomenon*; i.e., it is triggered by the current density reaching a "supercritical" value J^* . This statement also pertains to the BS model, which assumes the LO approach though extending the LO validity by accounting for the quasiparticles heating. In fact, there are more current-based explanations for the jump other than LO+BS, as the pair-breaking or depairing current limit,¹⁴⁻¹⁷ the heated electron model (at low temperatures),¹⁸ or vortex depinning at twin boundaries.²¹

An opposite view for the voltage jump is the thermal view. This is a broad issue that needs going some more deeply into it. A starting observation is that the always non-vanishing measuring time leads to temperature-increasing experimental CV curves from otherwise constant-temperature CVCs. A thermal origin for the voltage jump is realized if at a given temperature reached during the CV measuring run, the system can no longer keep its thermal balance stable and so undergoes a temperature runaway. The voltage jump would be thus *temperature driven*. Note that it is not to be understood that the superconductor should reach a high temperature and by no means the critical temperature. In fact, according to experimental data,^{10,22} if one is to explain the observed jump by thermal instability, no more than 2-3 K overtemperature (with respect to that of the bath) should suffice to trigger the thermal runaway. The thermal balance is complex and involves input power, power increase rate with temperature, measuring time (this one having a direct bearing on the overheating), thermal coupling of the film to the substrate, thermal conductivity of the substrate's material, and so on.

A central question is how current-driven and temperature-driven effects acting on the experimental CV curves can be discriminated or, if both exist, how can be separated. This question translates into other one; what are the constant-temperature CV characteristics of $\text{YBa}_2\text{Cu}_3\text{O}_{7-\delta}$ like? (Of course we are referring to the ideal, strictly constant temperature, curves not to the experimental ones.) A first possibility is that they vary smoothly with current in which case the experimental voltage jump can only arise by a thermal runaway due to the finite measuring times. In the second case, namely, current itself triggering the jump, there would be a competition of effects. From the premise that thermal effects are unavoidable, in this paper we explore the first possibility.

Thermal analysis on the CV characteristics in superconductors is of course no novelty and quite a few are available. Most of them however have been applied to the study of propagation of normal zones in the sample (usually monitored by voltage taps set along the sample)^{10,15,23–25} and to hysteresis.^{26–28} In these works no question is made on the causing mechanism of the initial normal zone or, say, the highly dissipative state, but instead the focus is on its propagation. These approaches are consistent as the samples under study are “by definition” inhomogeneous, the inhomogeneity being either created artificially or as obtained, in this latter case often associated with a large sample’s length.

Regarding the “homogeneous” thermal approaches to the quench in high- T_c superconductors, fewer are known to us. It is worth commenting on the contribution from Kiss *et al.*²⁹ They give a semiquantitative explanation of the observed quench in $\text{YBa}_2\text{Cu}_3\text{O}_{7-\delta}$ films and Bi-based coils. Key concepts such as positive feedback, instability criterion based on the temperature derivative of power (not on power itself), catastrophic transition point, etc., are placed on the foreground. The main limitation is perhaps the use of a zero-dimensional heat equation for the calculation of the film’s temperature along the CV curve.

An improved thermal model was proposed, few years ago, by Viña *et al.*³⁰ that solved the temperature field in the film and its substrate altogether. This model was based on one uniform-temperature domain whose boundary expanded at the diffusion length rate with some correction for the film’s temperature. A jumping current density, J^* , was predicted that agreed with experiments to within 10%–20% but the agreement for the electric field at and before the jump was poor. In spite of the model’s crudeness, it allowed us to explain very recent measurements showing a decrease in the quench current J^* with increasing film’s width.³¹ In all, though these findings show the adequacy of a thermal runaway to explain the observed voltage jump, a convincing quantitative analysis accounting of both jump quantities J^* and E^* is still lacking, at least within the same degree as the current-driven theories.

This paper develops a finite-element method (FEM) analysis aiming at assessing whether sensible noncritical, namely, smooth, constant-temperature CV curves may show up as the singular quasidiscontinuous curves the experimentalist measures. Special attention will be given to the role of the measuring time and the sample geometry. The results from the simulation will be compared to experimental results from $\text{YBa}_2\text{Cu}_3\text{O}_{7-\delta}$ films of different widths and resistivities

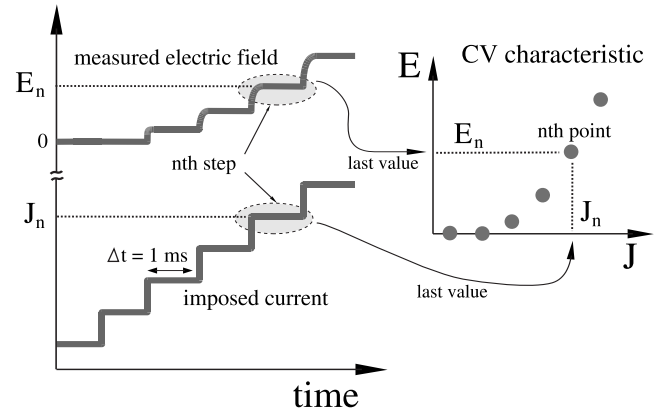


FIG. 1. Experimental building procedure of the current-voltage characteristics studied in this work. A staircase ramp of current was applied to the $\text{YBa}_2\text{Cu}_3\text{O}_{7-\delta}$ microbridges. Each current step was applied for 1 ms. Voltage data were subsequently acquired at a rate of 10^5 samples/s resulting in a slightly rounded voltage step. 50 current steps were applied in each run with a current increase between steps from 2 to 10 mA.

using a measuring scale on the millisecond range under self field. The use of FEM is advisable because it yields accurate simulations on the physics response over complex geometries, is capable of dealing with nonlinearity, and is widely available. Moreover, with FEM analyses the role of any conceivable variable in the (here) thermal process, from the substrate’s thermal conductivity or environment exchange coefficient to the film’s width or the measuring pulse duration, can be studied.

II. EXPERIMENTAL DETAILS

The CV data utilized in this work were measured from various microbridges. As complete details about fabrication and general characteristics of the samples have been already published,^{30,31} only the minimum information will be given here. The microbridges are from epitaxial $\text{YBa}_2\text{Cu}_3\text{O}_{7-\delta}$ thin ($0.15 \mu\text{m}$) films grown onto $\text{SrTiO}_3(100)$ substrates either by pulsed laser ablation or by sputtering techniques. Their widths range from 10 to $100 \mu\text{m}$ with an aspect ratio, i.e., length to width, of about 10. No magnetic field was applied.

Since heating effects simulations must match the experimental conditions, specially the run time, a description of the experimental procedure is in order. Our CV curve measurements are current driven via stepped ramps with about 1 ms duration steps. Sample voltage was measured with a data-acquisition card, getting the full CV curve in typically 30 ms. The sample holder was exposed to a He gas atmosphere inside a temperature-regulated cryostat. As illustrated in Fig. 1, each plateau pair from the current vs time and voltage vs time curves determines a point in the CV characteristic; in fact only the last point from both plateaus were used. Needless to say that the CV curve so obtained is not a constant-temperature curve but rather a temperature-increasing CV curve. The temperature of the lower-current points corresponds closely to that of the bath. We will take advantage of this feature later on to build sensible constant-temperature curves.

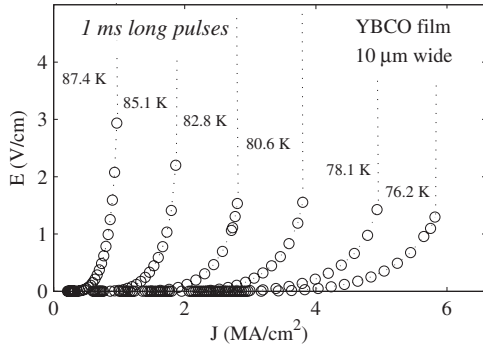


FIG. 2. Experimental data for one of the $\text{YBa}_2\text{Cu}_3\text{O}_{7-\delta}$ microbridges whose $T_c=89.9$ K. Six bath temperatures are drawn. More series were measured but are not shown for the sake of clarity. No data points above the jump are shown because the factor of 50 discontinuities in voltage would downplay the most relevant lower data points.

Figure 2 shows some representative data sets at six temperatures of CVCs so obtained. No data points after the jump are shown since the factor of around 50 jump in the electric-field values would have minimized the data points before the jump. Notwithstanding, these high-field data may be seen elsewhere,³² and an example of the whole voltage range is depicted at the inset of Fig. 7. These data are quite similar to other data already published for high- T_c films^{2,26,30,33} at zero applied magnetic field.

III. FINITE-ELEMENT METHOD APPROACH

As already anticipated, our aim here is to assess whether the jump itself is a thermal effect and secondarily what fraction of the voltage measured along the whole CV curve of $\text{YBa}_2\text{Cu}_3\text{O}_{7-\delta}$ films is due to the heating effects arising from Joule power. A straightforward procedure for this is as follows: one would undertake subtracting the overheating from the measured electric field so as to obtain the ideal or intrinsic, i.e., strictly constant temperature, CV curves. Unfortunately, this direct way is not tractable because the actual film's temperature at each current should be known but its accurate measurement is hardly feasible and only indirect and semiquantitative results are available.^{10,22} We are thus compelled to go the other way around.

The two main steps in the implementation of this reverse way are as follows. The starting point is as just said presuming the constant-temperature CVCs. For that end, the low-current experimental data points will be the “anchor” from which those CVCs will be built. Next, solve the thermal dissipation problem accounting for the experimental conditions, i.e., applying the current (in the simulations) following the experimental pace. The process requires a previous compilation from the literature of the various thermal intervening parameters. Of course the hard step is the solving of the thermal problem as it involves a nonlinear system (the electric field depends nonlinearly on current density and temperature). A description of the details goes next.

A. Obtaining the constant-temperature characteristics

We want here to build sensible constant-temperature CVCs compatible with the experimental data. This compat-

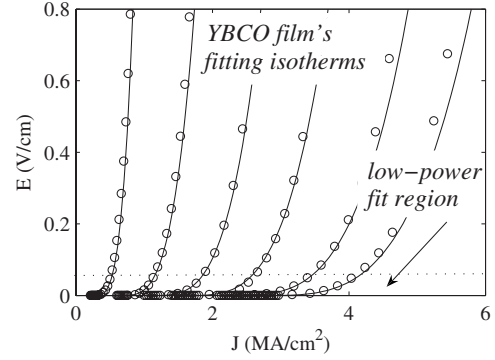


FIG. 3. Low-voltage range for the same experimental data as Fig. 2. The solid lines are the constant-temperature CVCs we will be using along this paper as the *background* CVCs (for this sample), obtained from the fit of the functional form in Eq. (1) over the indicated voltage region (below the dotted line). These isothermal CVCs are smooth all along the current range up to the normal state.

ibility translates into requiring a good accord to the low-current data points where the actual sample's temperature can well be identified with the bath's temperature. For the general structure of the constant-temperature CVCs we will use the functional form,

$$E(J, T) = E_0(T) \left[\frac{J}{J_0(T)} - 1 \right]^n, \quad (1)$$

where

$$E_0(T) = E_1 \left(1 - \frac{T}{T_c} \right)^{n_0}, \quad (2)$$

$$J_0(T) = J_1 \left(1 - \frac{T}{T_c} \right)^{n_0}, \quad (3)$$

with E_1 , J_1 , n_0 , and n taken as constant free parameters. Equation (1) applies in the case $J \geq J_0$, whereas $E(J, T) = 0$ for $J \leq J_0$.

The above functional form which may be termed critical power law has been obtained as certain limits arising in: (i) the weak pinning flux-creep context,¹⁵ (ii) the mean-field approximation in the strong pinning limit,^{34,35} and (iii) granular behavior models.³⁶ Note that we do not ascribe to the critical power law a more fundamental or central physical significance than we do to other alternative models for CVCs found in the literature. The critical power law serves us well in that: (i) it fits quite well to the low-current experimental data over the whole range of temperatures and (ii) it extrapolates smoothly to higher currents. These features are illustrated in Fig. 3 where it can be seen that the goodness of fit over the fit region is quite high at any temperature. The lower limit of the fit region is understandably the critical current J_c . The setting of the upper limit for current is a more delicate issue. Since the fit region should be the heat-free portion of the CVC, the upper current should correspond to the higher current for which, within experimental uncertainties, no temperature rise takes place. For that, the “heated version” of the constant-temperature CVCs must be first calculated (this is

in fact our main task in this paper) and then by comparison between both sets of curves the current at which departure starts off is determined. If this departure current is higher than the upper fit current the latter is increased, repeating the loop until both currents are brought to coincidence. In summary, the upper fit current is obtained by a self-consistent method. The assumed constant-temperature CVCs, of which Fig. 3 is an example, are smoothly varying in both current and temperature, and we can term them heat-free or simply isothermal CVCs.

The isothermal CVCs may be interpreted as the curves an experimentalist using very fast equipment would measure. How fast should that measurement rate be? The faster the better, but with the limit of the electronic response time. Experimental work shows that the resistive switching of $\text{YBa}_2\text{Cu}_3\text{O}_{7-\delta}$ microbridges occurs after a delay time of 10–20 ns.^{37,38} Response times of a few nanoseconds have been also reported by studying $\text{YBa}_2\text{Cu}_3\text{O}_{7-\delta}$ films sensitivities to subnanosecond infrared and optical pulses.^{39–41} However, no agreement seems to exist as to which response components are bolometric, i.e., electronic, or nonbolometric, i.e., thermal. Anyhow, this time threshold thus sets the ideal measurement rate; in numbers, the whole CVC curve should be measured in approximately (50 current steps) $\times (10 \text{ ns/step}) = 500 \text{ ns}$ to guarantee the minimum thermal effects, but no such experimental results are known to us. We are thus faced with the key question posed above. Assuming the ideal or constant-temperature CVCs of $\text{YBa}_2\text{Cu}_3\text{O}_{7-\delta}$ microbridges are like those seen in Fig. 3 as solid curves, what would be like the “apparent” CVCs measured when using 1-ms-long or 1- μs -long current pulses? Would they resemble those actually measured? Only through appropriate thermal calculations can we give an answer. Sections III B 1 and III B 3 describe the calculation systematics.

B. Finite-element method details

Our $\text{YBa}_2\text{Cu}_3\text{O}_{7-\delta}$ microbridges are 0.15 μm thick spanning 10–100 μm in width. Their length was varied to keep a fixed aspect ratio of 10; i.e., the microbridges’ length was systematically ten times their width. The intended purpose was to use a two-dimensional (2D) modeling thus much alleviating the numerical burden of simulations. The FEM implementation of our 2D film-substrate system involves a number of steps, the most important of which are as follows.

1. Meshing film and substrate

Though meshing is done automatically by any FEM package it is not always so when there are geometric regions with highly different sizes. In our case, the $\text{YBa}_2\text{Cu}_3\text{O}_{7-\delta}$ microbridge’s cross section is typically $10 \times 0.15 \mu\text{m}^2$ and $5 \times 1 \text{ mm}^2$ for the substrate. These dimensions fix the maximum finite-element size to 0.15 μm , giving about 2×10^8 elements in all. This is still a huge number even halving the system (simulation of either the right-side half or the left-side half of the film-substrate ensemble can be done without any loss of generality). The way out of this is using an inhomogeneous meshing finer at the film (a finite-element size of 0.15 μm is appropriate here) and coarser as we deepen into

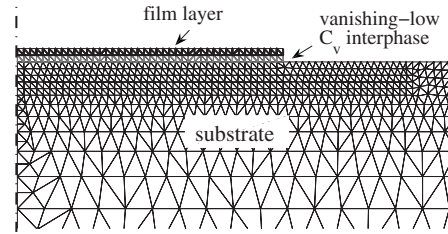


FIG. 4. Illustration of the meshing build for one of the $\text{YBa}_2\text{Cu}_3\text{O}_{7-\delta}$ thin films. Note that by taking advantage of the left-right symmetry, only the right half of the film is modeled. Because of the tiny size of the film with respect to the substrate an inhomogeneous meshing was needed to save degrees of freedom.

the substrate. This was carried out by building rectangular regions expanding from the film’s location and setting the meshing density at the boundary closer to the film finer than the density at the father side. Figure 4 is a snapshot of the meshing process illustrating the increasing finite-element size as getting farther from the film.

2. Boundary conditions and materials properties

A proper thermal parameters’ choice is important for an approach intending to provide absolute magnitudes on the $\text{YBa}_2\text{Cu}_3\text{O}_{7-\delta}$ films’ CVCs without fitting parameters. As for the SrTiO_3 substrate, the values $C_p = 1 \text{ J/K cm}^{-3}$ and $\kappa_s = 0.18 \text{ W/K cm}$ will be used.⁴² For the film-substrate exchange coefficient the value $h_{fs} = 10^3 \text{ W/K cm}$ is found.^{43–45} The temperature gap at the film-substrate interface was implemented through a very thin *ethereal* medium, i.e., having a vanishing low specific heat and the precise thermal conductivity to simulate the correct boundary impedance. In Fig. 4 it can be seen the low- C_v buffer layer at the bottom of the film representing the film-substrate thermal impedance.

The film exchanges heat with its surrounding coolant (nitrogen gas in our case) as well. By using general correlations for flat heaters exchanging with their coolant gas,⁴⁶ we obtain $h_{sg} = 2 \times 10^{-3} \text{ W/K cm}$. The fact that the substrate-gas interface is around 6 orders of magnitude less efficient than the film-substrate interface makes irrelevant the environment heat exchange at short enough times, as experimental work supports.¹⁷ The environment is expected to become a factor in the thermal analyses when the diffusive heat front reaches the substrate’s boundary. In the millisecond range the thermal diffusion length is around 250 μm , not reaching then the substrate boundary (1 mm thickness). However, at longer measurement times, say, in the hundreds of milliseconds, thermal environment should be more determinant, as also confirmed by experimental work.⁴⁷ Anyhow, h_{sg} will be included in the simulations as it adds no special complication to the FEM machinery. As advanced above, only half of the film-substrate system will be simulated since its mirror image can be accounted for by setting no heat exchange at the cutoff section, this section being coincident with the symmetry plane.

3. Thermal load

It is the term giving account of how much heat is produced in the film. In our current transport setup heat is pro-

duced by the Joule power (volume) density $Q=EJ$. A uniform current density across the film will be assumed for $J > J_c$. An explicit support for current homogeneity comes from the work of Herrmann *et al.*,^{48,49} as they identify in high- T_c tapes a characteristic current above which additional current is distributed homogeneously across the entire superconductor's cross section. Interestingly, this cutoff current is slightly below the critical current. Direct measurements by a microarray of Hall probes laid onto Bi-based crystals show that current flows along the sample edges at relatively low temperature ($T \lesssim 50$ K) but nonuniformity becomes negligible above relatively near T_c ($T \gtrsim 80$ K).⁵⁰ Further evidence rests with more recent work on $\text{YBa}_2\text{Cu}_3\text{O}_{7-\delta}$ strips carrying transport current.⁵¹ Here by using magneto-optical imaging it is observed that even at a low temperature of 20 K and $I/I_c=0.9$, the nonuniformity of J is only of the order of 20%. Finally, let us point to a number of works supporting the independence of critical current on bridge width.^{12,31,52,53} Without a claim for exclusivity the simplest explanation is current flowing uniformly distributed throughout the whole sample's cross section.

Under a uniform current density J the local dissipating power $Q=EJ$ can only depend on local temperature, J only changing discretely at each current switch. We are then left with a biunivocal power-temperature relationship as $Q(T)=E(J_i, T)J_i$, where J_i is the value of the pulse current applied at step i . From this a thermal load table $(T, J_i) \rightarrow Q$ can be built, which values will act as the heat sources in the film's time evolution simulation. Notice that the electric field in the heat generation rate $E(J_i, T)J_i$ is not of course the experimental field at $J=J_i$ since we do not know which temperature the sample has but the electric field at $J=J_i$ for the isothermal CVC at the calculated temperature T (this is the core of the thermal feedback).

C. Calculation systematics

With all the above ingredients the thermal numerical calculations can proceed, an illustration of which is shown by the flow diagram on Fig. 5. In words, the main steps are as follows.

(a) The YBCO film-substrate system starts off a well-defined initial state: an applied current $J_i=J_c$ (there is no dissipation below J_c) and a temperature $T_i=T_{\text{bath}}$.

(b) The sample is heated at a rate $Q(T_i, J_i)$ for a time δt much less than the pulse duration t_{pulse} . Their ratio determines the accuracy of results; we chose it as 1/40.

(c) A temperature map $T_o(x, t)$ is then provided by the finite-element method.

(d) Time is raised in δt , temperatures updated, and the thermal load $Q(T_i, J_i)$ is recalculated, with which a new iteration begins. The (injected-heat) \rightarrow (resulting-temperature-field) calculation loop continues until current time reaches the pulse duration. Only the temperature map at the end of the pulse life is recorded in order to match our experimental conditions.

(e) A new current pulse is fed to the film by raising the current density, $J_i \rightarrow J_i + \delta J$. As no delay between pulses is allowed, the initial temperature distribution (initial condi-

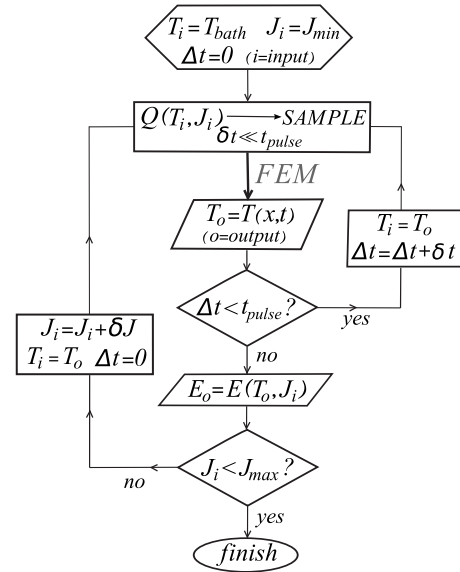


FIG. 5. Block diagram illustrating the main steps in the FEM thermal analysis of the $\text{YBa}_2\text{Cu}_3\text{O}_{7-\delta}$ film.

tions) is set to the final temperature distribution of the previous current pulse.

(f) The outer loop continues until a preset maximum current J_{max} is reached. Typically 50 current steps were used to build the whole CVC. This final current was chosen to be above the experimental J^* .

The outcome for each loop is the temperature profile at the end of the current pulse, namely, the temperature at each of the finite-element nodes. It has been checked that temperature differences in the film are bounded by one- or two-tenths of kelvins, the difference being maximum between the film's center (hotter) and edges (cooler), as one would expect. We are then entitled to assign a unique temperature, namely, the average temperature, to the whole film, results on which will be presented in Sec. IV.

IV. RESULTS FROM THE FINITE-ELEMENT METHOD CALCULATIONS

In this section a systematic presentation of the main results from the FEM analysis on the thermal behavior of YBCO films will be accomplished. We will focus on those FEM predictions for which experimental counterpart exists. These measurements are basically the CVCs themselves at different temperatures and film widths.

A. Probing the jump in temperature

According to our thermal calculation route (see Fig. 5) the quantity directly obtained is the film's temperature as a function of current. Pertaining results are illustrated in Fig. 6. In this figure it is shown the temperature evolution of a YBCO film subjected to increasing current and starting from three bath's temperatures, namely, 85.1, 80.6, and 76.2 K, as labeled at the respective curves' foot. The most singular feature is the occurrence of a temperature discontinuity a few kelvins above the bath's temperature, as illustrated by the

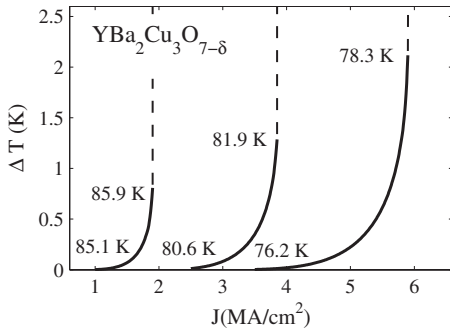


FIG. 6. FEM simulation results for the YBCO film’s temperature evolution. The three curves show the film’s differential temperature (relative to that of the bath) for three initials bath’s temperatures as a function of current density. The important result is the appearance of a numerical instability in the film’s temperature slightly above the bath’s temperature. The jump in temperature in these simulations is of tens of kelvins, leading the sample to the normal state.

breakage of the solid lines in Fig. 6. Thermal-only calculations reproduce then an abrupt jump of some tens of kelvins (the above-jump temperatures, not illustrated, are within normal-state temperatures). Note also that the triggering temperature for the discontinuity is less than 3 K above the bath’s temperature, in close agreement with the available data already addressed to in Sec. I.^{10,22} As film’s temperature is not a measurable quantity no comparison is possible with experiments. However, corresponding simulation results for the electric field are indeed susceptible of comparison, which task is undertaken in Sec. IV B.

B. Comparison of the current-voltage thermal-only FEM simulations with experimental results

In this section we translate the results from Sec. IV A, namely, sample’s temperature as a function of current density, into a form more susceptible of being tested experimentally. If we remember the isothermal curves conjectured for the film’s behavior, i.e., Eq. (1), the transformation $(T, J) \rightarrow (E, J)$ is just an algebraic formality. Figure 7 shows a typical example of a FEM simulation with the experimental data points.

The results from Fig. 7 are perhaps the most important contribution from this study because it shows how smooth and so jump-free constant-temperature CVCs may manifest themselves as an abrupt CVC when the sample is subjected in the simulations to a relatively slow (1 ms) staircase current ramp that clones the one experimentally used in our measurements (on the other hand a most common measurement rate, see Sec. I).

On its way toward the thermal runaway the sample crosses successive isotherms. This is illustrated in Fig. 8 where the simulation not only shows again the excellent FEM result for the jump current but also shows how the film’s temperature drifts from the bath’s to the quenching temperature $T^*=81.5$ K. The overall predictions of the FEM thermal-only simulations are condensed in Fig. 9. There the whole temperature measuring range for one of our 10 μm

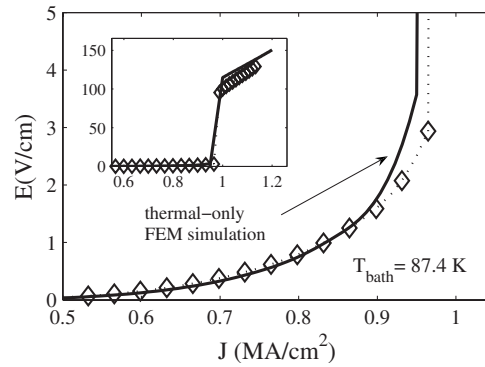


FIG. 7. Comparison between measurements of the current-voltage curves (diamond symbols) and the calculations based only on thermal effects sketched in Fig. 5 (solid lines). These data correspond to the bath temperature $T=87.4$ K. Current is applied in the simulations by staircase ramps of 1 ms duration per step to match experimental conditions. The agreement is good, giving in particular a 1.5% deviation for J^* and around of 16% for E^* . The inset shows an overview of the same comparison, here including the landing into the normal state. Note the huge discontinuity in the electric field.

film is subjected to comparison. The agreement with the FEM results is outstanding, reinforcing the thermal origin of the voltage jump in superconducting YBCO films.

The cautious reader may wonder about the tricks of this trade. Once a set of isothermal CVCs are assumed the FEM outcome is a no-free-parameter calculation as detailed above. By this statement we meant that the (thermal) parameters values are set prior to the comparison with the data. This differs by example from what is customarily made when analyzing CVCs in terms of the LO theory, where the critical vortex velocity (or equivalently the inelastic-scattering time) is left as a free parameter.^{1–13} The greater source of uncertainty is linked with the constant-temperature CVCs themselves. As graphically illustrated in Fig. 3 there is a choice to make, setting aside the functional form, as to the experimental data entering the fit. In Fig. 3 the threshold field was taken slightly below 0.1 V/cm following the criteria invoked in Sec. III A. What would have been the simulation results say for a threshold of 0.2 or 0.02 V/cm? From our experience

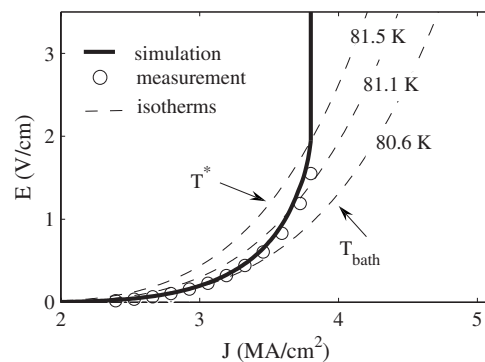


FIG. 8. Detailed view of one of the CVC of our 10- μm -wide film showing the drift in temperature as current is fed into the sample. The film crosses successive isotherms (three of them are illustrated) until thermal instability triggers the voltage jump.

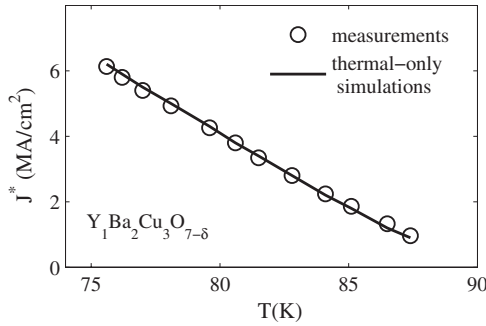


FIG. 9. Experimental data of the instability current J^* for the whole range of measuring temperatures of a $10\ \mu\text{m}$ width YBCO film. The solid line is the thermal-only FEM simulations from the jump-free CVCs of Fig. 3. The calculation error is approximately equal to the data points' size.

we would state that an uncertainty of around 5% in J^* may be associated with the isothermal CVCs choice. In summary, the data point diameter is a sensible estimate for the jump current J^* calculation error in Fig. 9. However suggestive the excellent agreement may seem, in our view the main contribution of this paper is not the quantitative account of measurements but the fact that when heat production is not neglected and neither the experimental measuring pace, the observed voltage discontinuity is closely reproduced in FEM simulations. In other words, the former two factors are essential and not accidental in the proper analysis.

Though the essential achievements of the FEM-based thermal model for the voltage jump in YBCO films is summarized in Figs. 7–9, additional experimental test is possible when considering other film parameters. This is the case of film's width which is a thermal parameter. By this statement we mean that in the (typical) micrometer range no other relevant superconducting length as the coherence length or the magnetic penetration depth can get comparable values, and thus film's width should be in principle a neutral or irrelevant parameter. However from the thermal point of view widths in the $10\text{--}100\ \mu\text{m}$ range are comparable with the thermal diffusion length whose value is around $200\ \mu\text{m}$ at the millisecond time range. Size effects have been in fact studied quite recently.³¹ It is worth notwithstanding revisiting the issue in the light of FEM calculations.

The capabilities of the FEM method are illustrated in Fig. 10 where the CVCs of two films of quite different width are compared. The electric field has been normalized to the corresponding prior-to-jump experimental value E^* because of their big difference: $0.052\ \text{V/cm}$ for the $100\ \mu\text{m}$ film and $2.61\ \text{V/cm}$ for the $10\ \mu\text{m}$ film. Except for their width these two films are closely similar in their intrinsic properties such as thickness or normal resistivity, whereby in the absence of thermal effects they should exhibit the same J^* .

It may be enlightening to briefly argue why, as data points show, wider films are more thermally unstable than the narrower ones. The simple idea is that the narrow films are more *edgy* than wider films and so have more substrate volume available to get thermally balanced. For our quasi-one-dimensional films, i.e., $w(\text{width}) \gg d(\text{thickness})$ the characteristic length is played by the thickness d . Because of that

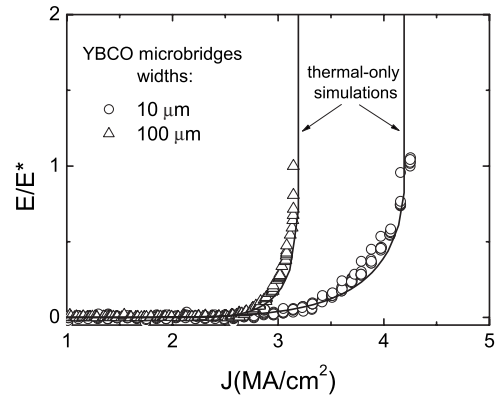


FIG. 10. Comparison of the voltage jump for two YBCO films of quite different width but otherwise the same normal-state resistivity. Their critical temperatures are $88.15\ \text{K}$ ($100\ \mu\text{m}$ film) and $87.20\ \text{K}$ ($10\ \mu\text{m}$ film). The distinct jump current is accounted for by the same thermal-only FEM simulation. The common bath temperature is $78.1\ \text{K}$.

one could expect that the edge region would extend a distance d from the edge itself. In other words the edge or say the outer points of a film are $2d$ in width, whereas the inner points are $w-2d$. The ratio (outer points)/(inner points) $\approx 2d/w$ clearly favors the narrow films as thermal stability is concerned.

Note finally the excellent agreement FEM thermal-only calculation achieves for the observed behavior (see Fig. 10). Additional simulations show that the width bearing on thermal stability greatly drops at bigger widths ($w \geq 100\ \mu\text{m}$). This is not only confirmed experimentally³¹ but it is also understandable from the above discussion: the edge region loses relevance since all points tend to be inner points as width grows.

V. DISCUSSION AND CONCLUSIONS

The FEM-based results presented above for YBCO films show that (isothermal) conventional flux-creep, i.e., smooth, CVC are quantitatively compatible with the abrupt quasi discontinuous CVCs experimentalists measure. Considering that only the inevitable heating effects have been computed to obtain the actual electric field, one is forced to recognize that the observed transition to a highly dissipative state in YBCO films is thermal in origin. In other words, the system abruptly switches into the normal state because of a thermal instability caused by the heat fueled by the electric current density. It is the actual temperature and thermal power that determines the voltage instability not current itself. Note that by construction our system obeys jump-free isotherms; i.e., there is no electrical current able to provoke by itself an electric-field discontinuity at any constant temperature.

A first delicate-to-deal-with conclusion is that in order to explain the voltage jump in Y-based superconductors under our experimental conditions, no contribution from vortex instabilities such as the Larkin and Ovchinnikov (LO) theory or other current-driven explanations (see Sec. I) was needed. This means that under certain circumstances the *natural*

heating effects take the lead and avoid those current-driven mechanisms to emerge. It is thus important to remember which are those experimental conditions.

Our measurements are restricted to temperatures relatively near T_c whereby any phenomenology pertaining to $T \ll T_c$ is in principle excluded. Besides, no magnetic field was applied. In the eventual competition of both mechanisms magnetic field is perhaps a key factor. On one side, the influence of any model relying on vortex instabilities (LO) should by force be enhanced by a magnetic field as it is a vortex generator. On the other side, we have found difficulties in fitting unpublished experimental results on YBCO films under magnetic field to a purely thermal model (assuming as in here uniform currents).

Refrigeration conditions should be another key factor in the relevance of thermal instability. For instance, our samples are grown onto SrTiO₃ substrates, but MgO substrates, having a thermal conductivity about ten times larger, are used quite as often. One could also have easily films half as thick as ours or have a factor of 2 better heat transfer coefficient to the substrate. Still within standard specifications one could end up with 40 times more effective cooling. It is quite straightforward to perform a FEM analysis under these quite different thermal conditions. Referring to the results in Fig. 9 we have found that J^* could rise in around 50%. In other words, the thermal instability would be considerably delayed in current but will not be inhibited by the better refrigeration conditions.

A way out of this competition between intrinsic and non-intrinsic causes for the voltage jump can come from experi-

ments using increasingly short measuring times. Thermal effects should certainly be minimized at shorter measuring times, which opens the possibility of viewing other underlying effects. Some experimental data at low magnetic field are available³³ that show a smearing out of the voltage jump when shortening from 100 ms to 50 μ s the current pulse duration, suggesting that there is nothing beyond thermal effects. However further experimental work will be welcome to elucidate this important issue.

Our results do not close down the issue of thermal stability on these complex systems. FEM, or more generally numerical, calculations do not give any clue as to why does the voltage jump occur. In this regard questions as to under what temperature and dissipated power does thermal runaway get triggered or what is the influence of thermal history on thermal instability need methods beyond numerical ones. We think that only analytical work can lead to understand thermal behavior by predicting the stability and instability *regions* of high- T_c superconductors so as to tailor their behavior to practical purposes as it could be the case of film-based current limiters. This theoretical path is presently being undertaken.

ACKNOWLEDGMENTS

This work has been supported under Projects No. 2006/XA049 and No. 07TMT007304PR (XUGA-FEDER) and by Project No. FIS2007-63709 (MEC-FEDER). G.F. acknowledges financial support from Spanish Ministerio de Educación y Ciencia through a FPI grant.

*fmmaza@usc.es

¹W. Klein, R. Huebener, S. Gauss, and J. Parisi, *J. Low Temp. Phys.* **61**, 413 (1985).

²Z. L. Xiao and P. Ziemann, *Phys. Rev. B* **53**, 15265 (1996).

³Z. L. Xiao, E. Y. Andrei, and P. Ziemann, *Phys. Rev. B* **58**, 11185 (1998).

⁴Z. L. Xiao, P. Voss-de Haan, G. Jakob, T. Kluge, P. Haibach, H. Adrian, and E. Y. Andrei, *Phys. Rev. B* **59**, 1481 (1999).

⁵S. G. Doettinger, R. P. Huebener, R. Gerdemann, A. Kühle, S. Anders, T. G. Trauble, and J. C. Villègier, *Phys. Rev. Lett.* **73**, 1691 (1994).

⁶S. Doettinger, R. Huebener, S. Kittelberger, and C. Tsuei, *Europhys. Lett.* **33**, 641 (1996).

⁷F. Lefloch, C. Hoffmann, and O. Demolliens, *Physica C* **319**, 258 (1999).

⁸F. Kamm, A. Pettl, and P. Ziemann, *Physica B (Amsterdam)* **284-288**, 561 (2000).

⁹M. Pauly, R. Ballou, G. Fillion, and J. C. Villègier, *Physica B (Amsterdam)* **284-288**, 721 (2000).

¹⁰M. Decroux, L. Antognazza, N. Musolino, E. de Chambrier, S. Reymond, J. Triscone, F. Fisher, W. Paul, and M. Chen, *IEEE Trans. Appl. Supercond.* **11**, 2046 (2001).

¹¹D. Babic, J. Bentner, C. Sürgers, and C. Strunk, *Phys. Rev. B* **69**, 092510 (2004).

¹²M. N. Kunchur, B. I. Ivlev, D. K. Christen, and J. M. Phillips,

Phys. Rev. Lett. **84**, 5204 (2000).

¹³C. Peroz and C. Villard, *Phys. Rev. B* **72**, 014515 (2005).

¹⁴S. Reymond, L. Antognazza, M. Decroux, E. Koller, P. Reinert, and O. Fischer, *Phys. Rev. B* **66**, 014522 (2002).

¹⁵L. Antognazza, M. Decroux, S. Reymond, E. de Chambrier, J. Triscone, W. Paul, M. Chen, and F. Fisher, *Physica C* **372-376**, 1684 (2002).

¹⁶M. N. Kunchur, C. Wu, D. H. Arcos, B. I. Ivlev, E. M. Choi, K. H. P. Kim, W. N. Kang, and S. I. Lee, *Phys. Rev. B* **68**, 100503(R) (2003).

¹⁷J. E. McCrone, J. L. Tallon, J. R. Cooper, A. C. MacLaughlin, J. P. Attfield, and C. Bernhard, *Phys. Rev. B* **68**, 064514 (2003).

¹⁸M. N. Kunchur, *Phys. Rev. Lett.* **89**, 137005 (2002).

¹⁹M. Noe and M. Steurer, *Supercond. Sci. Technol.* **20**, R15 (2007).

²⁰I. Kolmakov, E. Vernoslova, K. Titkov, and M. Sitnikova, *Physica C* **372-376**, 562 (2002).

²¹P. Bernstein, J. Hamet, M. González, and M. Ruibal, *Physica C* **455**, 1 (2007).

²²L. Antognazza, M. Decroux, N. Musolino, J.-M. Triscone, P. Reinert, E. Koller, S. Reymond, M. Chen, W. Paul, and O. Fischer, *J. Low Temp. Phys.* **117**, 1543 (1999).

²³A. Lehner, A. Heinrich, K. Numssen, and H. Kinder, *Physica C* **372-376**, 1619 (2002).

²⁴G. D. Poulin, J. Lachapelle, S. H. Moffat, F. A. Hegmann, and J.

- S. Preston, *Appl. Phys. Lett.* **66**, 2576 (1995).
- ²⁵V. Meerovich, V. Sokolovsky, M. Gladstein, and S. Shtutina, *Physica C* **366**, 291 (2002).
- ²⁶T. Peterson, I. Maartense, and R. R. Biggers, *IEEE Trans. Appl. Supercond.* **5**, 1436 (1995).
- ²⁷M. Tinkham, J. U. Free, C. N. Lau, and N. Markovic, *Phys. Rev. B* **68**, 134515 (2003).
- ²⁸W. Skocpol, M. Beasley, and M. Tinkham, *J. Appl. Phys.* **45**, 4054 (1974).
- ²⁹T. Kiss, M. Inoue, K. Hasegawa, K. Ogata, V. Vyotky, Y. Ilyin, M. Takeo, H. Okamoto, and F. Irie, *IEEE Trans. Appl. Supercond.* **9**, 1073 (1999).
- ³⁰J. Viña, M. T. González, M. Ruibal, S. R. Currás, J. A. Veira, J. Maza, and F. Vidal, *Phys. Rev. B* **68**, 224506 (2003).
- ³¹M. Ruibal, G. Ferro, M. R. Osorio, J. Maza, J. A. Veira, and F. Vidal, *Phys. Rev. B* **75**, 012504 (2007).
- ³²J. Viña, Ph.D. thesis, Universidade de Santiago de Compostela, 2003; arXiv:cond-mat/0305712v2 (unpublished).
- ³³G. Jakob, P. V. de Haan, M. Wagner, Z. Xiao, and H. Adrian, *Physica B (Amsterdam)* **284-288**, 897 (2000).
- ³⁴V. F. Solovjov, V. M. Pan, and H. C. Freyhardt, *Phys. Rev. B* **50**, 13724 (1994).
- ³⁵D. S. Fisher, *Phys. Rev. B* **31**, 1396 (1985).
- ³⁶M. Prester, *Supercond. Sci. Technol.* **11**, 333 (1998).
- ³⁷K. Harrabi, N. Cheene, F. Chibane, F. Boyer, P. Delord, F.-R. Ladan, and J. Maneval, *Supercond. Sci. Technol.* **13**, 1222 (2000).
- ³⁸G. Sabouret, C. Williams, and R. Sobolewski, *Phys. Rev. B* **66**, 132501 (2002).
- ³⁹W. Donaldson, A. Kadin, P. Ballentine, and R. Sobolewski, *Appl. Phys. Lett.* **54**, 2470 (1989).
- ⁴⁰A. Frenkel, M. Saifi, T. Venkatesan, P. England, X. Wu, and A. Inam, *J. Appl. Phys.* **67**, 3054 (1990).
- ⁴¹G. L. Carr, M. Quijada, D. B. Tanner, C. J. Hirschmugl, G. P. Williams, S. Etemad, B. Dutta, F. DeRosa, A. Inam, and T. Venkatesan, *Appl. Phys. Lett.* **57**, 2725 (1990).
- ⁴²*Thermophysical Properties of Matter*, edited by Y. Touloukian (Plenum, New York, 1970), Vols. 2 and 5.
- ⁴³M. Nahum, S. Verghese, P. Richards, and K. Char, *Appl. Phys. Lett.* **59**, 2034 (1991).
- ⁴⁴C. Marshall, A. Tokmakoff, I. Fishman, C. Eom, J. M. Phillips, and M. Fayer, *J. Appl. Phys.* **73**, 850 (1993).
- ⁴⁵B. Li, L. Pottier, J. Roger, and D. Fournier, *Thin Solid Films* **352**, 91 (1999).
- ⁴⁶A. Bejan and A. D. Kraus, *Heat Transfer Handbook* (Wiley, New York, 2003).
- ⁴⁷C. Villard, C. Perez, B. Guinard, and P. Tixador, *IEEE Trans. Appl. Supercond.* **15**, 11 (2005).
- ⁴⁸J. Herrmann, N. Savvides, K. Müller, R. Zhao, G. McCaughey, F. Dermann, and M. Apperley, *Physica C* **305**, 114 (1998).
- ⁴⁹J. Herrmann, N. Savvides, and K. Müller, *IEEE Trans. Appl. Supercond.* **9**, 1824 (1999).
- ⁵⁰D. T. Fuchs, E. Zeldov, M. Rappaport, T. Tamegai, S. Ooi, and H. Shtrikman, *Nature (London)* **391**, 373 (1998).
- ⁵¹A. Bobyl, D. Shantsev, Y. Galperin, T. Johansen, M. Baziljevich, and S. Karmanenko, *Supercond. Sci. Technol.* **15**, 82 (2002).
- ⁵²R. Hahn, G. Fotheringham, and J. Klockau, *IEEE Trans. Appl. Supercond.* **5**, 1440 (1995).
- ⁵³R. B. Dinner, K. A. Moler, D. M. Feldmann, and M. R. Beasley, *Phys. Rev. B* **75**, 144503 (2007).